A&A 402, L17–L20 (2003)
DOI: 10.1051/0004-6361:20030448

Astronomy & Astrophysics

Slow-mode standing waves observed by SUMER in hot coronal loops

T. J. Wang, S. K. Solanki, D. E. Innes, W. Curdt, and E. Marsch

Max-Planck-Institut für Aeronomie, 37191 Katlenburg-Lindau, Germany

Received 12 March 2003 / Accepted 25 March 2003

Abstract. We report the first detection of postflare loop oscillations seen in both Doppler shift and intensity. The observations were recorded in an Fe XIX line by the SUMER spectrometer on SOHO in the corona about 70 min after an M-class flare on the solar limb. The oscillation has a period of about 17 min in both the Doppler velocity and the intensity, but their decay times are different (i.e., 37 min for the velocity and 21 min for the intensity). The fact that the velocity and the intensity oscillations have exactly a 1/4-period phase difference points to the existence of slow-mode standing waves in the oscillating loop. This interpretation is also supported by two other pieces of evidence: (1) the wave period and (2) the amplitude relationship between the intensity and velocity are as expected for a slow-mode standing wave.

Key words. Sun: corona – flares – oscillations – UV radiation

1. Introduction

In recent years, high temporal and spatial resolution space telescopes have led to significant progress in observations of coronal MHD waves. For example, kink mode oscillations excited by flares in coronal loops were detected by TRACE in EUV radiation (Nakariakov et al. 1999; Aschwanden et al. 1999; Aschwanden et al. 2002). Slow magnetosonic waves were observed in cool coronal loops by SOHO/EIT (e.g. Berghmans & Clette 1999; De Moortel et al. 2002). These observations allow MHD waves to be used for coronal seismology (e.g. Nakariakov & Ofman 2001) and are important for developing wave-based theories of coronal heating.

Very recently, the Solar Ultraviolet Measurements of Emitted Radiation (SUMER) spectrometer on SOHO discovered damped oscillations of hot coronal loops in Doppler shift (Kliem et al. 2002; Wang et al. 2002a–c, 2003). Observations of 27 flare-like events show that the oscillations have periods in the range of $P = 7{-}31$ min and decay times of $\tau_{\rm d} = 6{-}37$ min. The observed strong decay has been explained in the context of a 1D MHD model as a consequence of thermal conduction acting on the slow mode oscillations by Ofman & Wang (2002). In this study, we report convincing evidence that these Doppler oscillations are caused by slow-mode standing waves in coronal loops.

2. Observations

A class M1.2 flare occurred at the north-west limb on 15 April 2002. The flare began at 23:05 UT and peaked at 23:24 UT in GOES 1–8 Å X-ray flux. SUMER observed this flare with the $300'' \times 4''$ slit placed at a fixed position in the corona above the flaring active region (see Fig. 1). The spectra were recorded with a 50 s cadence in three lines: S III λ 1113.2 (0.03–0.06 MK), Ca X λ 557.7 (2nd order, 0.7 MK), and Fe XIX λ 1118.1 (6.3 MK). For each line, the window of the recorded spectra has a range of 2.2 Å. A single Gaussian was fitted to the line profiles to obtain a Doppler shift time series at each spatial pixel (see Fig. 2a). The Fe XIX line exhibits not only strong brightenings lasting several hours, but also distinct regions of coherent oscillations along the slit. For two such regions, we average over a width of 6 pixels ($\sim 1''$ pixel^{-1}) to get an average time profile. The function

$$V(t) = V_0 + V_{\rm m}\sin(\omega t + \phi)\mathrm{e}^{-\lambda t}, \quad (1)$$

is then fitted to the Doppler oscillation, where V_0 is the background shift, $V_{\rm m}$ is the amplitude and ω, ϕ, and λ are the frequency, phase, and decay rate, respectively.

3. Results

The flare was observed by EIT in the 195 Å channel. There were a few images around flare onset, and then a data gap of 2 hours. EIT observing resumed again around 2:00 UT. SUMER observations were continuous and registered the cooling of postflare loops from 6.3 MK (Fe XIX) to 0.03 MK (S III). Similar cooling features are also observed in another event by TRACE and SUMER (Wang et al. 2002d). There were two distinct loop systems (marked A and B in Fig. 1). Figures 1a,b show the evolution of Fe XIX and S III intensity at the height of the SUMER observations. For both loop systems

Send offprint requests to: T. J. Wang,
e-mail: wangtj@linmpi.mpg.de

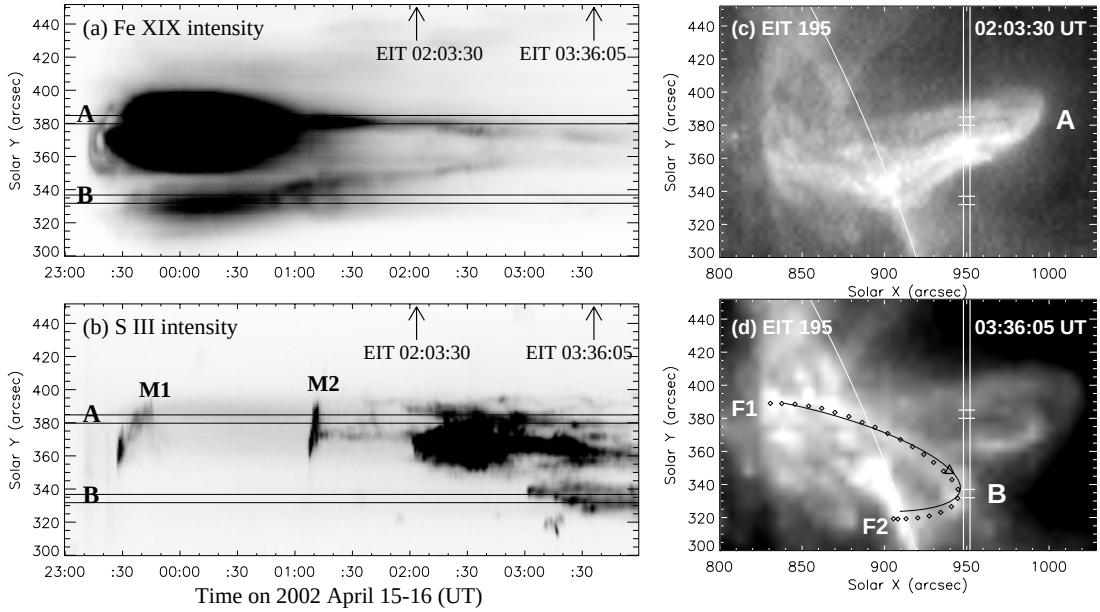

Fig. 1. Observations of a M1.2 flare on 2002 April 15. **a), b)** Line-integrated intensity time series at a fixed slit position. The labels A and B mark strips with equal widths of 6 pixels along the slit. **c), d)** EIT 195 Å images. The times at which they were recorded are marked by arrows at the top of **a)** and **b)**. The SUMER slit is indicated as two vertical lines, and positions of two cuts (denoted A and B in **a)** and **b)**) are marked. In **d)** a candidate of the oscillating loop (outlined with *diamonds*) is fitted with a circular model (dark curve). The apex position of the modelled loop is marked by a *triangle*.

the S III emission appears several hours later at the same location as the Fe XIX, indicating that the magnetic structure in the coronal arcades remains unchanged as the plasma cools. This is also supported by the fact that twice transient northward-moving brightenings (marked M1 and M2 in Fig. 1b) occurred at the same location along the slit as system A. The EIT image at 2:03 UT (Fig. 1c) shows that the SUMER observations of system A were taken about half way up the loop arcade. The plasma in system B was not observed in the EIT 195 Å channel until about 3:00 UT. SUMER was observing near the top of this system (Fig. 1d).

Doppler oscillation events are found to occur twice at two regions near the cuts A and B, respectively (see Fig. 2a). At the start of both oscillation events cool plasma ejection was seen in S III (Fig. 1b). This suggests that the oscillations are probably excited by small aftermath events near a loop footpoint. We will study in detail the trigger of these events in the next paper.

In this study, we concentrate only on the oscillation features at region B. The geometrical parameters of loop B can be determined from the EIT image in Fig. 1d, assuming a loop with a circular shape and using the same method as in Aschwanden et al. (2002). The azimuth angle of the loop baseline to the east-west direction is $\alpha = 19°$. The inclination angle of the loop plane southward to the vertical is $\theta = 27°$. The loop length is derived as $L = 191$ Mm and the length of the segment BF2 is $L_{\rm BF2} = 64$ Mm, i.e. $L_{\rm BF2} = (1/3)L$. The angle between the line-of-sight and the magnetic field (assuming it to point toward the footpoint F1) near cut B is $\gamma = 15°$.

The first oscillation event began at about 23:30 UT, still during the Fe XIX brightening phase. This oscillation is strongly damped with a period of 16 min and a decay time of 11.4 min. The later event began at 0:50 UT in the flare decay phase. Strikingly, the line-integrated intensity around cut B shows periodic fluctuations overlaid on a decreasing background (see Fig. 2c). In order to see the intensity oscillation more clearly, we subtract the background trend, obtained by temporally smoothing the intensity series (see Fig. 2b).

Of particular interest is the second oscillatory event, which lasted for about 100 min. During this time more than 5 periods of Doppler and intensity oscillations were detected (see Figs. 3a,b). We measure physical parameters of the oscillations from the best fit damped sine function (see Eq. (1)). For the Doppler oscillation we obtain an amplitude of $V_{\rm m} = 18.0 \pm 1.5$ km s^{-1}, a period of $P = 17.6 \pm 0.1$ min, and a decay time of $\tau_{\rm d} = 1/\lambda = 36.8 \pm 2.6$ min. A ratio of $\tau_{\rm d}/P \gtrsim 2$ is unique among the coronal oscillations seen by SUMER so far, $\tau_{\rm d}/P \simeq 1$ being more typical (Wang et al. 2003). For the intensity oscillation we analyze the difference profile (see Fig. 3b), which is derived by subtracting a 20-pixel (≈17 min) smooth background trend. In this way we can separate the variation in intensity due to the oscillation from that due to the flare. Of advantage for this is the fact that the brightening due to the flare lasts much longer than the oscillation period. This is unusual for the brightenings associated with SUMER oscillations. We obtain an amplitude of $I_{\rm m} = (3.0 \pm 0.4) \times 10^{-2}$ W m^{-2} sr^{-1} and a relative amplitude of $I_{\rm m}/I(t_0) \simeq 0.19$ (where $I(t_0)$ is the background intensity at the start of the modeled time series). The intensity oscillation has a period of $P = 17.1 \pm 0.1$ min and a decay time of $\tau_{\rm d} = 21.0 \pm 1.6$ min. Within the errors the velocity and intensity periods are identical, but their decay times differ by a factor of about 2. Comparing the phase relation between the Doppler and intensity oscillations, we find that except for the first peak their phases differ by exactly a quarter of a period. This relation is characteristic of compressive standing

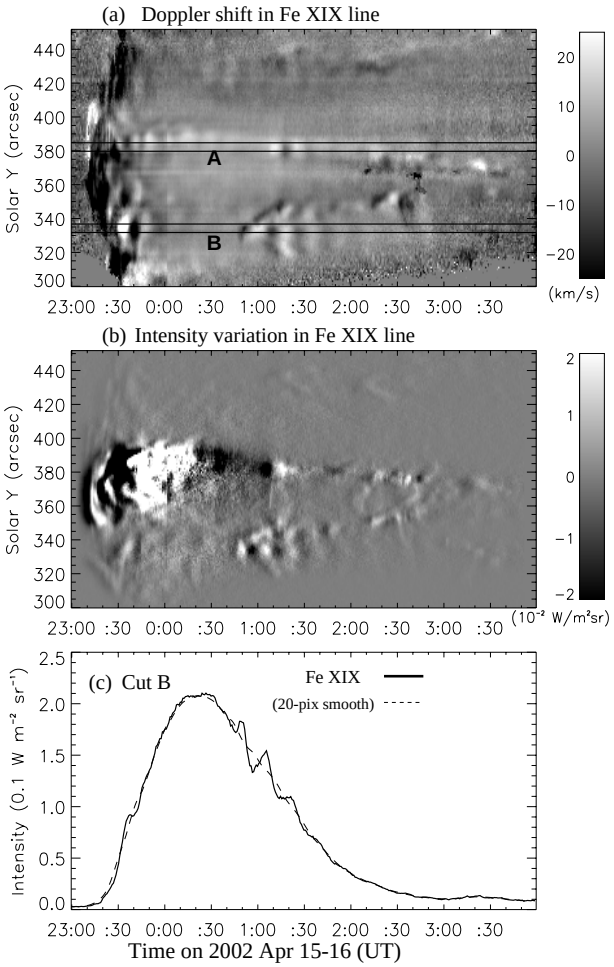

Fig. 2. a) Doppler shift time series at a fixed slit position. The redshift is represented with the bright color, and the blueshift with the dark color. The labels A and B mark strips with widths of 6 pixels along the slit. **b)** Line-integrated intensity time series with a removal of the background trend, which is taken as a temporal smoothing with a window of $\Delta t = 20$ pixels (~17 min). **c)** Time profiles of the Fe XIX line-integrated intensity for cut B, averaged along the slit within the two horizontal lines.

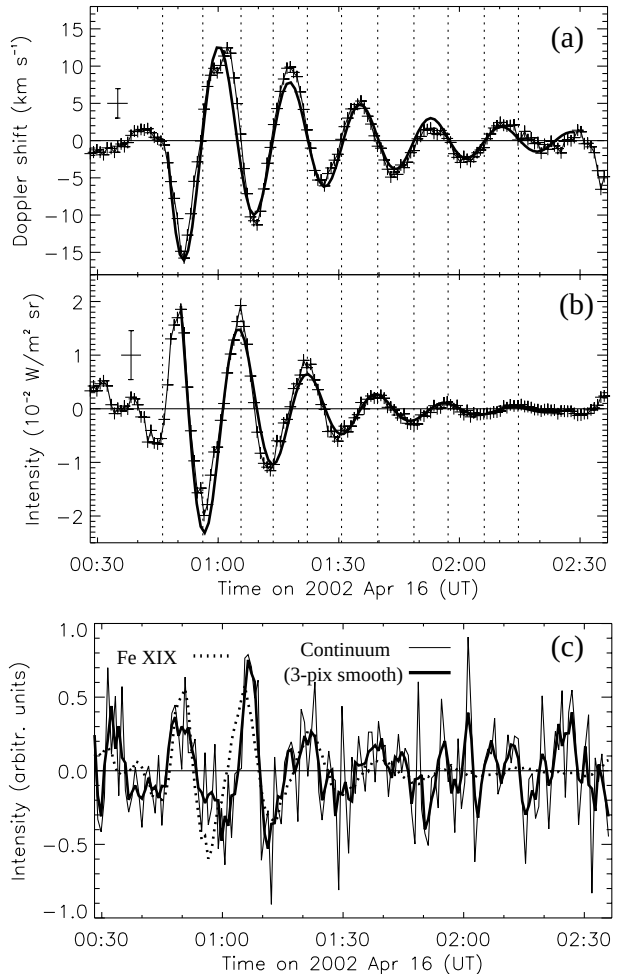

Fig. 3. a) Evolution of Doppler shift and **b)** of line-integrated intensity in the Fe XIX line for cut B. The thick solid curves are the best fits with a damped sine function. For the curves in **a)** and **b)**, the background shift (V_0 in Eq. (1)) and the background intensity have been removed, respectively. The error bars represent the standard deviation of shifts or intensities along the slit for cut B. **c)** Evolution of continuum intensity (thin solid curves), obtained by integration at the line wings of both S III and Ca X for cut B, and background removal similar as in **b)**. The thick solid curve is the 3-pixel smoothing of the thin one. As a comparison, the intensity curve of Fe XIX shown in **b)** is also plotted (dotted line).

waves (Sakurai et al. 2002; Ofman & Wang 2002). Figure 3c shows that in spite of considerable noise the continuum intensity shows quasi-periodic fluctuations, roughly in phase with the intensity oscillation in Fe XIX, giving further evidence for a compressive wave. Its peak at 01:06 UT displays a relative amplitude of about 0.08.

4. Discussion

We report several Doppler shift oscillation events in high (>6 MK) temperature postflare loops produced by a M-class flare recorded in an Fe XIX line by SUMER. We have analyzed in detail one of these cases, which was associated with periodic intensity fluctuations.

A large number of Doppler oscillation events were detected by SUMER (Wang et al. 2002b,c, 2003). Although some lines of evidence suggested slow standing waves as the cause of these oscillations, the absence of clear brightness fluctuations with the wave period argued against such an interpretation. The discovery of Doppler and intensity oscillations with the same period and an exact 1/4-period phase difference in this study gives us for the first time strong evidence in support of this idea.

For a standing slow mode wave $P_{\rm slow} \simeq 2L/c_{\rm s}$ (Roberts et al. 1984), where L is the loop length and $c_{\rm s}$ the sound speed. If we regard the loop seen by EIT as the oscillating loop, and assume that its geometry did not change much during its cooling, we obtain $P_{\rm slow} = 16.8$ min for this loop of $L = 191$ Mm with $T = 6.3$ MK (giving $c_{\rm s} = 380\,{\rm km\,s^{-1}}$). This result matches the observed period rather well.

To analyze the amplitude relationship between the velocity and intensity oscillations on the basis of the slow-mode waves,

we consider a damped standing wave of the following form for the velocity,

$$v(x,t) = V\cos(kx)\cos(kc_s t)e^{-\lambda t}, \quad (2)$$

where the magnetic field of the loop is taken to be along the x-direction, V is the amplitude and k is the wavenumber. The linearized continuity equation is

$$\frac{\partial \rho\prime}{\partial t} + \rho_0 \frac{\partial v}{\partial x} = 0, \quad (3)$$

where the disturbed density ρ is approximated by $\rho(x,t) = \rho_0 + \rho\prime(x,t)$, ρ_0 is the background density (a constant), and $\rho\prime$ the density perturbation. From Eqs. (2) and (3) we obtain

$$\frac{\rho\prime(x,t)}{\rho_0} = \frac{kV}{(k^2c_s^2+\lambda^2)^{1/2}}\sin(kx)\sin(kc_s t-\phi)e^{-\lambda t}, \quad (4)$$

where $\sin(\phi) = \lambda/(k^2c_s^2+\lambda^2)^{1/2}$. Allowing $V_x = V\cos(kx)$, from Eq. (4) we obtain a relationship between the density perturbation and velocity amplitude at position x along the loop,

$$\frac{\rho\prime}{\rho_0} = \frac{kV_x}{(k^2c_s^2+\lambda^2)^{1/2}}|\tan(kx)|. \quad (5)$$

For a fundamental mode, i.e. $k = \pi/L$ (consistent with the estimate for the wave period discussed above), we have $k^2c_s^2/\lambda^2 = 190 \gg 1$ for the observation, so that λ in Eq. (5) can be neglected. Thus, the amplitude of intensity oscillation, $\delta I/I$, and the amplitude of velocity oscillation along the loop have the following relation,

$$\frac{\delta I}{I} = \frac{2\rho\prime}{\rho_0} = \frac{2V_x}{c_s}|\tan(kx)|, \quad (6)$$

where the effect of temperature change on δI is neglected. For the intensity oscillations observed in Fe XIX, we measured $\delta I/I \simeq 0.19$. The line of sight amplitude $V_m = V_x\cos\gamma = 18.0\ \mathrm{km\,s^{-1}}$, with $\gamma = 15°$ (where γ is derived from the 3D loop geometry), so that $V_x = 18.6\ \mathrm{km\,s^{-1}}$. From Eq. (6) we obtain $|\tan(kx)| = 1.94$, then $x = 0.35\ L$ or $0.65\ L$. This expected position agrees with that derived from the 3D geometry for the position of cut B at the loop, i.e. $L_{BF2} = (1/3)L$. As a comparison, for a propagating wave, because the intensity and velocity variations are in phase, we can derive their amplitude relationship, $\delta I/I = 2V_x/c_s$, which is independent of position x along the loop. This relationship does not satisfy the observations. Therefore, estimates for both the wave period and the amplitude relationship of the intensity and velocity support slow standing waves in the loop as the source of the observed oscillations. For the relative intensity variation $\delta I(t)/I(t)$, in which the background trend $I(t)$ decreases with time (see Fig. 2c), we measured a decay time of $\tau_d \simeq 40$ min, close to the decay time of the Doppler velocity. This indicates that the relative amplitudes of the intensity variation and the Doppler velocity remain consistent with time.

The loop oscillation discussed in the present paper is particularly suited to reveal intensity oscillations, although we expect that they are present in other hot loop oscillations as well (the level relative to the velocity oscillations may change, however, as discussed above). Bumps in the intensity signal, which may be associated with the oscillations, are seen in many events (Wang et al. 2003). However, the combination of rapid damping of the oscillation and rapid change of the background intensity makes it extremely difficult to distill the intensity signal of the oscillations from the observations.

On the other hand, a kink-mode motion of the loop may also produce intensity and Doppler oscillations with possibly a 1/4-period phase difference when the slit is located at the loop top (see Fig. 1d). However, such an assumption will lead to a plasma β in the loop of about 2.4, which would be inconsistent with the usual coronal condition of low β. The same arguments against the kink wave interpretation for some other cases are also given by Wang et al. (2002a,c, 2003).

Wang et al. (2003) measured 54 Doppler oscillation cases in 27 events and found that the oscillations generally have a strong damping with $\tau_d/P \sim 1$ and the number of visible periods is less than 3. In this paper, however, the studied case is a unique one of the weakest damping (with 5 clearly visible periods and $\tau_d/P \gtrsim 2$) among all cases seen by SUMER so far. Based on MHD equations in Ofman & Wang (2002), we suggest that the weaker damping in this flare loop may be due to higher plasma density, possibly 1−2 orders of magnitude larger than that ($\sim 10^9\ \mathrm{cm^{-3}}$) in usual active region loops.

Acknowledgements. We would like to thank the referee Markus J. Aschwanden for his valuable comments. SUMER is financially supported by DLR, CNES, NASA and the ESA PRODEX programme. SOHO is a project of international co-operation between ESA and NASA.

References

Aschwanden, M. J., Fletcher, L., Schrijver, C. J., & Alexander, D. 1999, ApJ, 520, 880
Aschwanden, M. J., De Pontieu, B., Schrijver, C. J., & Title, A. 2002, Sol. Phys., 206, 99
Berghmans, D., & Clette, F. 1999, Sol. Phys., 186, 207
De Moortel, I., Hood, A. W., Ireland, J., & Walsh, R. W. 2002, Sol. Phys., 209, 89
Kliem, B., Dammasch, I. E., Curdt, W., & Wilhelm, K. 2002, ApJ, 568, L61
Nakariakov, V. M., Ofman, L., DeLuca, E. E., et al. 1999, Science, 285, 862
Nakariakov, V. M., & Ofman, L. 2001, A&A, 372, L53
Ofman, L., & Wang, T. J. 2002, ApJ, 580, L85
Roberts, B., Edwin, P. M., & Benz, A. O. 1984, ApJ, 279, 857
Sakurai, T., Ichimoto, K., Raju, K. P., & Singh, J. 2002, Sol. Phys., 209, 265
Wang, T. J., Solanki, S. K., Curdt, W., Innes, D. E., & Dammasch, I. E. 2002a, ApJ, 574, L101
Wang, T. J., Solanki, S. K., Curdt, W., et al. 2002b, in Proc. 11th SOHO Workshop: From Solar Minimum to Maximum, ed. A. Wilson (ESA SP-508, Noordwijk: ESA), 465
Wang, T. J., Solanki, S. K., Curdt, W., et al. 2002c, in Magnetic Coupling of the Solar Atmosphere, ed. H. Sawaya-Lacoste (ESA SP-505, Noordwijk: ESA), Proc. IAU Colloq., 188, 199
Wang, T. J., Solanki, S. K., Innes, D. E., & Curdt, W. 2002d, in (ESA SP-505, Noordwijk: ESA), Proc. IAU Colloq., 188, 607
Wang, T. J., Solanki, S. K., Curdt, W., et al. 2003, A&A, submitted